Journal of Power Sources 230 (2013) 25–31

Contents lists available at SciVerse ScienceDirect

Journal of Power Sources

journal homepage: www.elsevier.com/locate/jpowsour

Development and characterization of multilayered Cr–C/a-C:Cr film on 316L stainless steel as bipolar plates for proton exchange membrane fuel cells

Peiyun Yi [a], Linfa Peng [a], Tao Zhou [b], Hao Wu [a], Xinmin Lai [a,b,*]

[a] State Key Laboratory of Mechanical System and Vibration, Shanghai Jiao Tong University, Shanghai 200240, PR China
[b] Shanghai Key Laboratory of Digital Manufacture for Thin-walled Structures, Shanghai Jiao Tong University, Shanghai 200240, PR China

HIGHLIGHTS

- Cr–C/a-C:Cr film is deposited on SS316L sheet as bipolar plates using CFUBMSIP.
- Contact resistance is 2.89 mΩ cm^{-2} at 1.5 MPa and contact angle reaches 89.1°.
- The passivation current density is 0.276 μA cm^{-2} at 0.6 V in cathodic environment.
- Single cell with coated bipolar plate achieves peak power density of 1278.2 mW cm^{-2}.

GRAPHICAL ABSTRACT

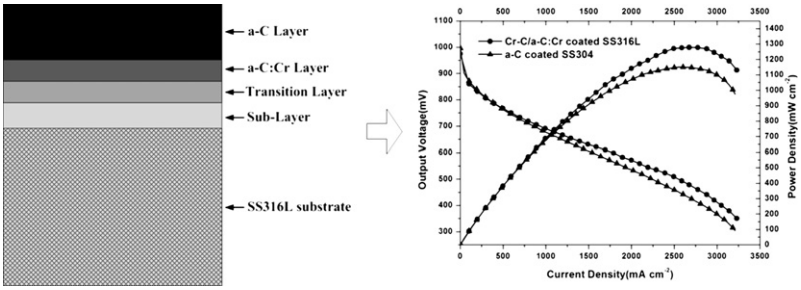

ARTICLE INFO

Article history:
Received 6 August 2012
Received in revised form
3 November 2012
Accepted 19 November 2012
Available online 10 December 2012

Keywords:
Proton exchange membrane fuel cells
Cr–C/a-C:Cr carbon film
Closed field unbalanced magnetron sputter ion plating
Performance

ABSTRACT

Multilayered chromium–carbon/amorphous carbon:chromium (Cr–C/a-C:Cr) is deposited on 316L stainless steel (SS316L) sheet as bipolar plates for proton exchange membrane fuel cells (PEMFCs) using closed field unbalanced magnetron sputter ion plating (CFUBMSIP). Raman spectra and X-ray diffractometry (XRD) indicate that the Cr–C/a-C:Cr film is composed of amorphous carbon, metallic Cr phase, chromium carbide phases. The stactic water contact angle of the film reaches 89.1°. Interfacial contact resistance (ICR) between the coated SS316L sheets and carbon paper is only 2.89 mΩ cm^2 at 1.5 MPa. Potentiodynamic tests in the simulated corrosive circumstance of PEMFCs reveals that the corrosion potential of coated samples is 0.236V *vs* SCE and the passivation current density is 0.276 μA cm^{-2} at 0.6 V in simulated cathodic environment. A single cell with Cr–C/a-C:Cr coated SS316L bipolar plates is assembled and tested to evaluate the *in-situ* performance of the film. The peak power density of the single cell is 1278.2 mW cm^{-2} at a current density of 2674.1 mA cm^{-2}. Compared to a-C coating developed in our previous work, the performance of Cr–C/a-C:Cr coating is improved in various aspects and Cr–C/a-C:Cr coated SS316L bipolar plates are more practically applied for commercialization of PEMFCs technology.

1. Introduction

Proton exchange membrane fuel cells (PEMFCs) attract more and more attention in recent years as a promising alternative clean power source for automotive and portable applications by virtue of its high-energy efficiency, pollution-free characteristics, relatively

* Corresponding author. State Key Laboratory of Mechanical System and Vibration, Shanghai Jiao Tong University, Shanghai 200240, PR China. Tel.: +86 21 34206303(office); fax: +86 21 34204542.
E-mail address: xmlai@sjtu.edu.cn (X. Lai).

0378-7753/$ – see front matter © 2012 Elsevier B.V. All rights reserved.
http://dx.doi.org/10.1016/j.jpowsour.2012.11.063

quick start-up, rapid response to varying loads, and low operating temperatures [1,2]. For a typical PEMFCs stack, the bipolar plate is a key component which accounts for approximately 80% of the stack volume, 70% of the stack weight and as much as 60% of the stack cost [3]. It serves for current conduction, heat dissipation, gas flow distribution and residual water removal, thereby directly influencing the fuel cell performance [4]. Stainless steel (SS) is a promising candidate material of bipolar plate because it permits plates as thin as possible and reduces stack volume and weight at a reasonable cost [5]. Nevertheless, it is widely recognized that even SS with passive oxide film on surface still suffers from corrosion in the harsh acidic and humid PEMFCs operation environment. Besides, the surface film significantly affects the contact resistance between the bipolar plate and the gas diffusion layer (GDL), and thus leads to power degradation [6]. So far, almost all SS substrates without any pretreatment could not achieve high electrical conductivity and high corrosion resistance simultaneously [7].

Depositing conductive and anticorrosive carbon film on SS substrate is a feasible and promising way to improve its interfacial contact resistance (ICR) and corrosion resistance using different methods. Antunes et al. [8] and de Oliveira et al. [9] reviewed major research topics and results in the corrosion protection and characterization of metal bipolar plates for PEMFCs. Different coating methods and substrate materials were addressed giving a comprehensive overview on carbon coated metal bipolar plates. Fukutsuka et al. [10] prepared a carbon coating on SUS304 using plasma-assisted chemical vapor deposition (CVD) method. The corrosion resistance of the bipolar plates was improved in simulated PEMFCs environments, and the ICR was also greatly reduced. Chung et al. [11] also evaluated the corrosion performance of carbon coated 304 stainless steel (SS304) bipolar plate. The carbon layer was produced via a thermal CVD method using a C_2H_2/H_2 mixed gas as carbon source. Depending on the acetylene to hydrogen ratio, the coating morphology varied from a filamentous porous layer to a continuous carbon coating. For the latter morphology the corrosion resistance was high enough to reach the performance of commercial pure graphite bipolar plate (Poco graphite). Fu et al. [12] found that a C–Cr composite coating greatly decreased the ICR and corrosion rate of 316L stainless steel (SS316L). They used a pulsed bias arc ion plating (PBAIP) deposition method which was chosen due to the low temperature, dense layer with few droplets that favor the final corrosion performance of the base metal. Afterwards, Wu et al. [13] also employed PBAIP technology to deposit a series of Cr containing carbon films on SS316L. X-ray photoelectron spectroscopy (XPS) and X-ray diffractometry (XRD) results indicated that the films were primarily composed of pure carbon atoms with amorphous structure, including sp^3 and sp^2 carbon atoms. The SS316L substrate coated with $Cr_{0.23}C_{0.77}$ film exhibited the lowest ICR and the highest corrosion resistance in simulated corrosive conditions of PEMFCs. Lee and Lim [14] developed a polymer composite of polyamide-imide filled with carbon black on stainless steel substrates using painting technology. The effects of the carbon black content on the ICR and corrosion resistance were investigated. The optimum carbon black content was about 40 wt.% taking the corrosion resistance and the contact resistance into account. Ren and Zeng [15] employed high-energy micro-arc alloying (HEMAA) technique to prepare compact titanium carbide as coatings for the type SS304 bipolar plates with a metallurgical bonding between the coating and substrate. It was found that TiC coating increased the corrosion potential of the bare steel in 1 M H_2SO_4 solution at room temperature by more than 200 mV, and decreased its corrosion current significantly. Wang et al. [7] developed a new metallic bipolar plates with pure graphite coating on metal substrates. The top layer was a continuous graphite sheet made by the expanded graphite flakes. The pure and layered graphite surface provides high electrical conduction and high chemical inertness in PEMFCs environments. There was a binder layer between the graphite sheet and the metal substrate, which mainly consisted of ester resin and conductive fillers. Potentiodynamic and potentiostatic tests conducted in simulated PEMFCs environments revealed the corrosion resistance of the graphite coated SS316L plates was greatly enhanced compared with the bare stainless steel substrate. Mori et al. [16] coated a conductive amorphous carbon (a-C) on the SUS316L separators by using an electron cyclotron resonance (ECR) plasma sputtering technique. The characterization of this carbon film suggested that the film was mainly composed of sp^2 and sp^3 bonding components. The contact resistivity between the coated SUS316L and carbon paper was found to be reduced by two orders of magnitude by the carbon coating. Show [17] prepared an a-C film on titanium bipolar plates at various temperatures by using the radio frequency plasma enhanced chemical vapor deposition (RF-PECVD) method. The results revealed that the a-C film coated titanium bipolar plates had lower ICR and the stack with the a-C coated Ti bipolar plates showed performance improvement. Feng et al. [18] and Jin et al. [19] investigated the performance of a-C coated SS316L and SS304 polished samples in a PEMFCs environment, respectively. They reported promising results of ICR and corrosion resistance under potentiodynamic and potentiostatic conditions. The dense and compact nature of the deposited film allied with the intrinsic high chemical stability and electrical conductivity of the carbon layer were responsible for the high desirable performance of the a-C coating. In our previous work [20], SS304 bipolar plates are fabricated by flexible forming process and a-C film is coated by closed field unbalanced magnetron sputter ion plating (CFUBMSIP). The initial performance of the single cell with a-C coated bipolar plates was 923.9 mW cm^{-2} at a cell voltage of 0.6 V, and the peak power density reached 1150.6 mW cm^{-2} at a current density of 2573.2 mA cm^{-2}. Performance comparison experiments between a-C coated and bare 304SS bipolar plates showed that the single cell performance was greatly improved by the a-C coating. Lifetime test of the single cell over 200 h and contamination analysis of the tested membrane electrode assembly (MEA) indicated that the a-C coating had excellent chemical stability.

As the continuation of the previous work, the present study deposits a multilayered chromium–carbon/amorphous carbon: chromium (Cr–C/a-C:Cr) on 0.1 mm thick SS316L sheet using CFUBMSIP to improve the performance and efficiency. The film characterizations are preliminarily evaluated by Raman spectra and XRD. Electric resistance including in-plane resistivity, through-plane resistivity and ICR is also investigated. Potentiodynamic and potentiostatic tests in the simulated corrosive circumstance of PEMFCs are conducted to evaluate the corrosion resistance of the coated SS316L samples. A single cell with Cr–C/a-C:Cr coated SS316L bipolar plates is assembled and tested to evaluate the *in-situ* performance of the film.

2. Experimental details

2.1. Sample preparation

Instead of polished samples [18,19], this study adopted commercial SS316L sheet with 0.1 mm in thickness as-received which is the raw material of stamped bipolar plates. The samples were cut into round with a diameter of 60 mm by wire Electrical Discharge Machining (EDM). Before coating, the round samples were carefully cleaned with acetone and distilled water by ultrasonic cleaning. The Cr–C/a-C:Cr film was then deposited on the round samples using a UDP850/4 CFUBMSIP system. Two 99.99%

chromium targets and two 99.99% graphite targets were used as sputtering source and high purity argon (99.99%) was used as the sputtering gases. To improve the adhesion strength between the substrates and the film, the substrates were firstly sputtered by plasma at a −700 V bias voltage to clean the substrate surfaces and obtain an active surface. The composition of Cr–C/a-C:Cr film is illustrated schematically in Fig. 1(a) and thickness of the Cr–C/a-C:Cr film was controlled by sputtering current as shown in Fig. 1(b). The coating process is mainly composed of the following four steps:

(1) The two Cr targets were firstly started to deposit a sub-layer only containing Cr. The sputtering current was increased to 5 A linearly in 1 min and then kept it for 4 min in stage (I).
(2) As a transition layer, the sputtering current of two chromium targets were decreased to 2 A and the sputtering current of two graphite targets were increased to 6 A gradually in 10 min in stage (II).
(3) The sputtering current of the chromium targets and graphite targets was kept at 2 A and 6 A for 60 min respectively to form a dense and compact a-C:Cr film in stage (III).
(4) The chromium targets was closed slowly in linear mode in 15 min, and the sputtering current of two graphite targets were kept at 5 A for another 45 min to form a-C film in stage (IV).

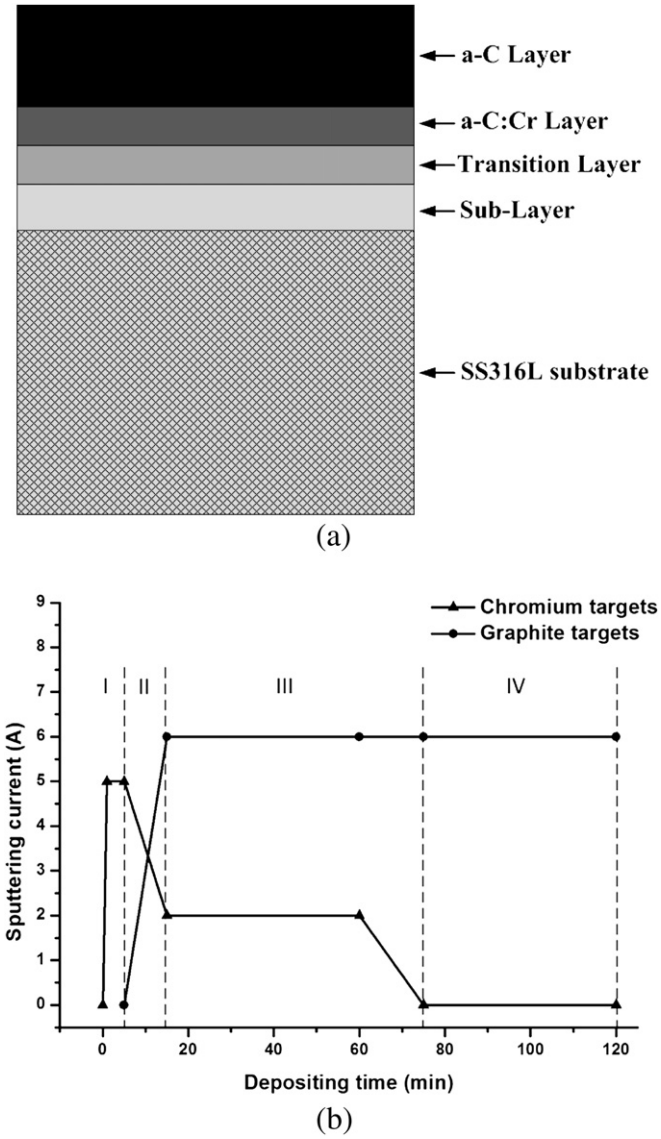

Fig. 1. Development of Cr–C/a-C:Cr film by CFUBMSIP (a) schematic of film composition (b) sputtering current control in the coating process.

2.2. Material characterization

The thickness of the Cr–C/a-C:Cr film on the SS316L samples was measured using a crater machine (BC-2, Teer Coatings, Ltd.) and calculated by the method well documented in the literature [19]. Surface morphology of coated samples was studied by a field emission scanning electron microscope (FE-SEM, FEI Sirion 200). The Raman measurements were performed to analyze the structural arrangement of carbon-based film using a Senterra R200-L Raman system (Bruker Optics, Germany). The excitation wavelength used was 514.5 nm from an Ar^+ laser [21]. The phase compositions of the as-prepared multilayered Cr–C/a-C:Cr films was identified through X-ray diffraction (XRD) patterns recorded by a D/MAX 2550 VB/PC diffractometer (Rigaku, Japan), using glancing angle technique with an incidence angle of 2°. Because hydrophobicity of bipolar plates can effectively influence the water management in a PEMFCs stack, the contact angle of the Cr–C/a-C:Cr SS316L with water was measured by OCA20 Optical Contact Angle Measuring Device (Dataphysics, Germany).

In-plane resistivity was measured by four-point probe technique with the probe diameter of 1.0 mm and the contact pressure of 1.2 MPa [22]. The ICR between Cr–C/a-C:Cr coated SS316L samples and GDL was measured by method well documented in the literatures [4,23] and experimental setups developed by our previous work [24]. Toray TGP-H-060 carbon paper, which was the same as that in MEA used in fuel cell performance evaluation experiments from Toray Industries, Inc., was adopted as simulated GDL. Besides, through-plane resistivity of bare and coated round samples were also measured using the same experimental setups at a compaction pressure of 1.5 MPa. Cr–C/a-C:Cr coated SS316L samples after potentiodynamic testing in simulated anodic and cathodic environment were also measured to investigate the influence of corrosion to ICR.

In order to evaluate the electrochemical behavior of the Cr–C/a-C:Cr coated SS316L samples, potentiodynamic and potentiostatic tests were carried out on a Corr-Test 150 Electrochemical Workstation and the electrolyte composition was 0.5 M H_2SO_4 solution with 5 ppm HF at 70 °C to simulate the aggressive PEMFCs environment [13]. Since the thickness of round samples was only 0.1 mm, a special fixture was designed, as shown in Fig. 2, to clamp the Cr–C/a-C:Cr coated SS316L sample with an exposed surface of 19.6 cm^2 (diameter of 5 cm). The backside was well sealed by two gaskets and connected to workstation as working electrode by a copper wire. After the potentiostatic test, the solutions were carefully collected and the concentration of metal ions Fe, Cr, Ni, Mo leached to solution due to corrosion was analyzed using inductively coupled plasma-mass spectrometry (ICP-MS, 7500a, Agilent Technologies Inc., USA).

2.3. Single cell assembly and tests

A self-developed single cell was designed and fabricated in house. The whole dimension of the bipolar plate is 150 mm × 100 mm × 1.2 mm with 45 serpentine flow channels to distribute reactant gas uniformly on the anode and cathode. The land width, channel width and channel depth of flow channels are 0.6 mm, 0.8 mm and 0.4 mm, respectively. The SS316L bipolar plates were fabricated by stamping process and bonded by laser welding process. Afterward, the bipolar plates were coated Cr–C/a-C:Cr film by CFUBMSIP system using the same parameters as SS316L round samples discussed above.

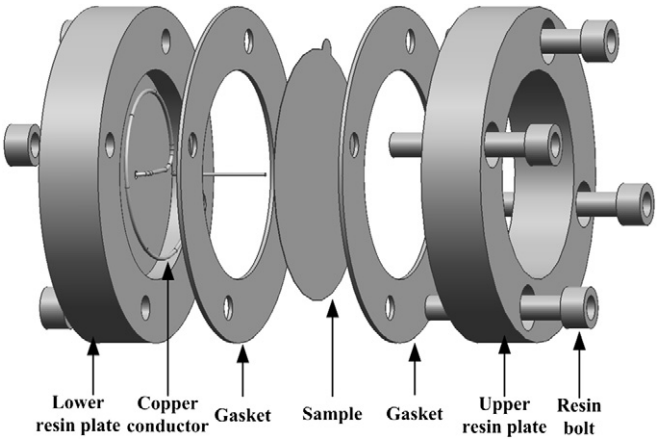

Fig. 2. Schematic of clamping fixture for potentiodynamic and potentiostatic tests of Cr–C/a-C:Cr coated 0.1 mm thick SS316L samples.

Commercial MEA with Nafion® 212 membrane in the thickness of 50 μm and platinum loading of 0.5 mg cm^{-2} for both the anode and cathode was adopted. The active electrode area is 82.56 cm^2 (9.6 cm by 8.6 cm). Aluminum plates in the thickness of 15 mm were used as the end plates and brass plates in the thickness of 2 mm were applied as the current collectors. Cr–C/a-C:Cr coated bipolar plates, MEA, silicon seals and current collectors were clamped between the two end plates by eight M4 screw joints with an assembly torque of about 6 Nm each. Cell temperature was maintained at 60 °C by adjusting the temperature of coolant water going through the centre of bipolar plate. The single cell performance was tested by measuring *I–V* curves with NBT-1000 fuel cell test system. The testing experiments were carried out using parameters presented in Table 1 under scanning current mode and the results were recorded after 1 h of stable operation.

3. Results and discussion

3.1. Cr–C/a-C:Cr film characterization

3.1.1. Phase analysis

Fig. 3 shows the thickness measurement results of the Cr–C/a-C:Cr film on SS316L sample. It is obvious that the total thickness of the Cr–C/a-C:Cr film is 1.411 μm, including a layer of 0.605 μm and another layer of 0.806 μm. However, it is hard to calculate the exact thickness of sub-layer, transition layer, a-C:Cr layer and a-C layer because there is no remarkable boundary between each layer.

Fig. 4 presents SEM images of a surface micrograph of the Cr–C/a-C:Cr film on SS316L sample in different magnitude. The transversal striations in Fig. 4(a) are attributed to the rolling trace of raw material because the samples are made of commercial SS316L sheet as-received without polishing. As shown in Fig. 4(b), no obvious pinhole is observed in our range of observation and the Cr–C/a-C:Cr film is dense, continuous and compact, indicating that the Cr–C/a-C:Cr film can block the substrate from direct corrosion.

Raman spectrum is an effective tool to characterize the structural arrangement of carbon atoms in carbon-based materials. The Raman spectra acquired from Cr–C/a-C:Cr coated SS316L sample

Table 1
Operating conditions for performance evaluation of single cell with Cr–C/a-C:Cr coated SS316L bipolar plates.

Active area	82.56 cm^2
Anode stoichiometric ratio	1.2
Cathode stoichiometric ratio	2.0
Anode pressure	0.3 MPa
Cathode pressure	0.3 MPa
Cell temperature	60 °C
Anode back pressure	30 kPa
Cathode back pressure	50 kPa
Hydrogen humidification	100%
Oxygen humidification	100%

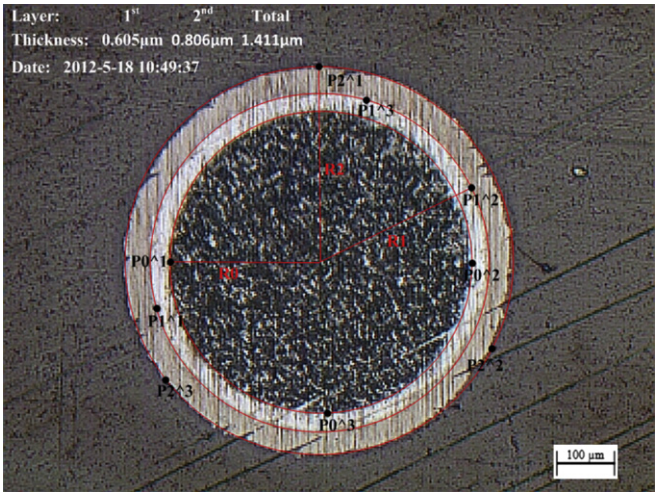

Fig. 3. Thickness measurement results of the Cr–C/a-C:Cr film on SS316L sample.

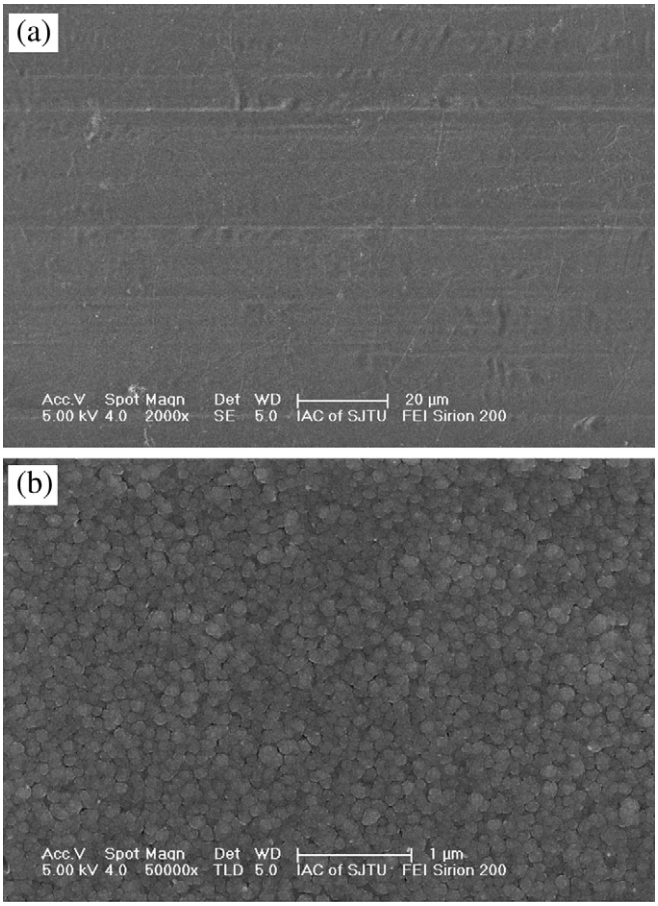

Fig. 4. SEM images of the surface micrograph of the Cr–C/a-C:Cr film on SS316L sample.

are designated to D and G peaks, which appear at 1380 and 1568 cm^{-1}, respectively [21]. The D peak is corresponding to disordered band (originating from the defects in the graphite crystal) and the G peak is due to the graphite band (originating from the graphite lattice). As shown in Fig. 5, the intensity of the D-band is higher than that of the G-band, indicating that the size of the disordered bands is larger than graphitic crystallites. This is typical characteristic of the amorphous carbon film [18].

Fig. 6 shows the glancing angle XRD patterns of the Cr–C/a-C:Cr coated SS316L sample which were collected at a glancing incidence angle of 2° to avoid the influences of the substrates of SS316L. In the recorded XRD patterns, the crystalline reflections are attributed to chromium crystallites and chromium carbide (Cr_3C_2 and Cr_7C_3) in the films, which is in good accordance with the results presented in the literatures [21,25]. By comprehensive consideration of Raman spectroscopy shown in Fig. 5, the film prepared by CFUBMSIP is composed of the amorphous carbon, metallic Cr phase, chromium carbide phases (Cr_3C_2 and Cr_7C_3).

3.1.2. Wettability characterization

The wettability of bipolar plate is considered to be a key parameter which greatly influences the efficiency of water management in a running PEMFCs stack especially at high current densities [12]. A high contact angle implies a high surface energy and would be helpful for water removal in the stack [26]. Fig. 7 shows the contact angle of the bare, a-C coated and Cr–C/a-C:Cr coated SS316L samples with water. To achieve an accurate value, three measurements are collected for each specimen. The average contact angle value of the bare and a-C coated SS316L samples are 73.2° and 78.8° [20], respectively, while that of Cr–C/a-C:Cr coated SS316L samples reaches 89.1°. These results demonstrate that the wettability characterization of SS316L is significantly improved by the Cr–C/a-C:Cr film. More importantly, the contact angle of Cr–C/a-C:Cr coated SS316L samples approaches 90° which is considered to be an ideal value to prevent accumulated water from flooding the electrode system [27].

3.1.3. Electric resistance

The in-plane and through-plane electric resistivity of bare and Cr–C/a-C:Cr coated SS316L samples were measured and the results are presented in Table 2. The in-plane resistivity of Cr–C/a-C:Cr coated SS316L is slightly higher than that of bare SS316L. The possible reason is that the surface layer of the carbon film contains

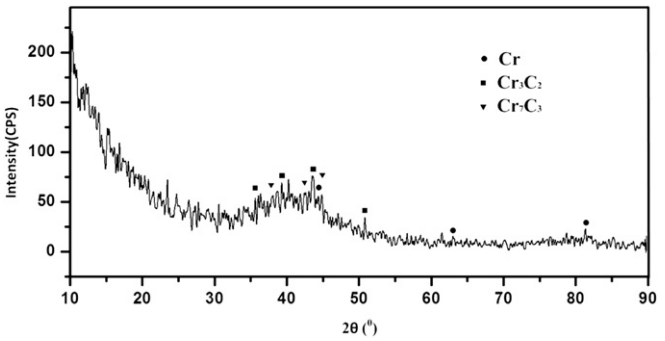

Fig. 6. Glancing angle X-ray diffraction patterns of the Cr–C/a-C:Cr coated SS316L sample.

numerous disarranged graphite structures and the resistivity of graphite is higher than SS316L [11]. Besides, the through-plane is also larger than bare SS316L. This phenomenon may be attributed to the fact that the sub-layer, transition layer, a-C:Cr layer and a-C layer are connected with SS316L substrate in series and there is an additive effect for electric resistivity. However, both the in-plane resistivity and through-plane resistivity are much lower than the Department of Energy's (DOE) 2020 technical target: $<1.0 \times 10^{-4}$ Ωm [28].

Actually, ICR between bipolar plate and GDL is a major factor affecting the cell performance than in-plane and through-plane resistivity in an operating PEMFCs [11]. The ICR of Cr–C/a-C:Cr coated SS316L samples with Toray TGP-H-060 carbon paper was measured at various compaction pressures .As shown in Fig. 8, the ICR decreases rapidly at low compaction pressures and then decreases gradually at high compaction pressures. At 1.5 MPa, the ICR of Cr–C/a-C:Cr coated SS316L is only 2.89 mΩ cm^2 which is lower than the DOE's 2020 technical target of 10 mΩ cm^2 [28], while the ICR of a-C coated SS316L is 5.4 mΩ cm^2 [20]. Fig. 8 also compares the ICR before and after potentiostatic testing in simulated anodic and cathodic environment. Significant change is not observed between the samples before and after potentiostatic testing and the slight difference may be caused by surface condition variance of raw material. Based on these results, it is concluded that the ICR of Cr–C/a-C:Cr coated SS316L was not affected by the polarization measurement in both anodic and cathodic environment [13].

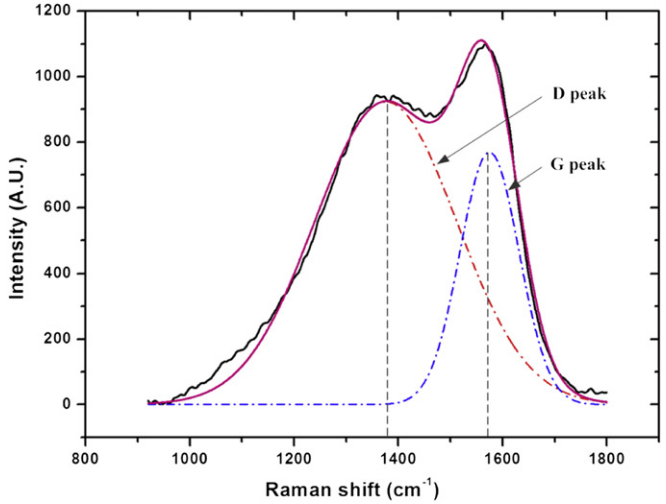

Fig. 5. Raman spectra of Cr–C/a-C:Cr coating on SS316L sample.

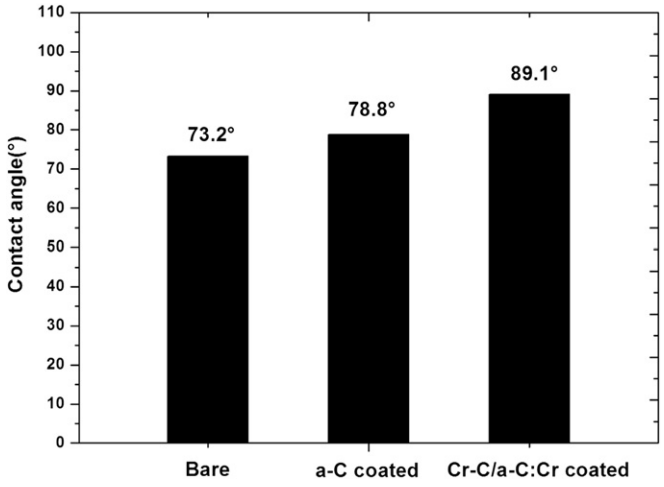

Fig. 7. Static water contact angle of bare, a-C coated and Cr–C/a-C:Cr coated SS316L samples.

Table 2
In-plane and through-plane electric resistivity of bare and Cr–C/a-C:Cr coated SS316L samples.

Bipolar plates	In-plane resistivity (Ωm)	Through-plane resistivity (Ωm)
Cr–C/a-C:Cr coated SS316L	7.85×10^{-7}	1.63×10^{-6}
Bare SS316L	7.50×10^{-7}	7.30×10^{-7}

3.1.4. Electrochemical behavior

In order to simulate the anodic and cathodic PEMFCs environments, the electrolytes were bubbled with 99.99% hydrogen and air, respectively. Fig. 9 shows the potentiodynamic polarization curves of a-C coated and Cr–C/a-C:Cr coated SS316L samples in the anodic and cathodic environments. Similar to a-C coated SS316L, there is no activation–passivation turning point for Cr–C/a-C:Cr coated SS316L in both anode and cathode environments. This phenomenon implies that there is no passive film formed on the sample surface and the material gets corroded continuously [4]. As shown in Fig. 9(a), the corrosion potential of Cr–C/a-C:Cr coated SS316L in anode environment is about 0.236 V *vs* SCE, which is more positive than the operation potential in the PEMFCs anode environment (around −0.1 V *vs* SCE) and a-C coated SS316L (around 0.2 V *vs* SCE) [20]. This is beneficial to retard the corrosion in the simulated and real anodic environment [18]. Besides, the corrosion potential in the cathodic environment, shown in Fig. 9(b), has the similar trend. The passivation current density of Cr–C/a-C:Cr coated SS316L in the cathodic operation potential (0.6 V *vs* SCE), which is marked with a vertical line in Fig. 9(b), is 0.276 μA cm^{-2}. Meanwhile, the current density determined from the a-C coated SS316L sample developed in our previous work is 3.56 μA cm^{-2}. Therefore, the corrosion resistance of Cr–C/a-C:Cr film is improved by an order of magnitude than a-C film and meets the DOE's 2020 technical target of 1.0 μA cm^{-2} [28].

The solutions after 10 h potentiostatic test were carefully collected and the concentration of metal ions dissolved due to corrosion was analyzed by ICP-OES. The contents of Fe, Cr, Ni, Mo, which are the major elements of SS316L, were recorded for bare, a-C coated and Cr–C/a-C:Cr coated SS316L samples in simulated anode and cathode environments and the results are presented in Table 3. The total metal ion concentrations leached from the bare SS316L sample is 7.957 ppm after 10 h potentiostatic test in the simulated PEMFCs cathode environments while this is only 0.4596 ppm for Cr–C/a-C:Cr coated SS316L. Compared to a-C coated sample, the metal ion concentrations of Cr–C/a-C:Cr coated SS316L is smaller and this trend is consistent with potentiodynamic results. Overall, the potentiodynamic and ICP results unequivocally indicate that the Cr–C/a-C:Cr coating improves the corrosion resistance of SS316L greatly.

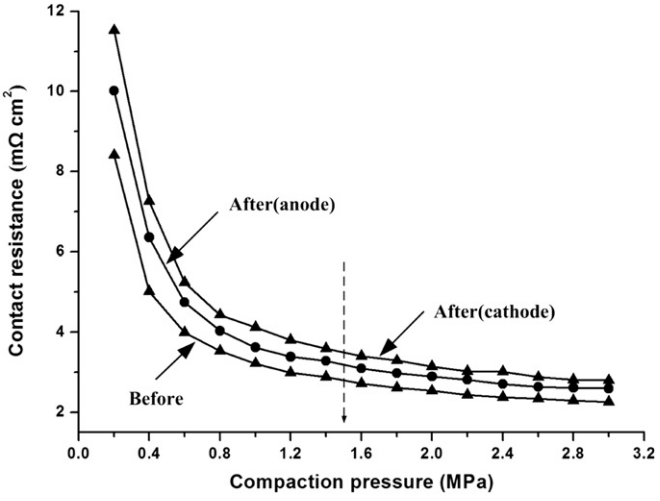

Fig. 8. ICR of Cr–C/a-C:Cr coated SS316L before and after potentiodynamic testing in simulated cathodic and anodic environment.

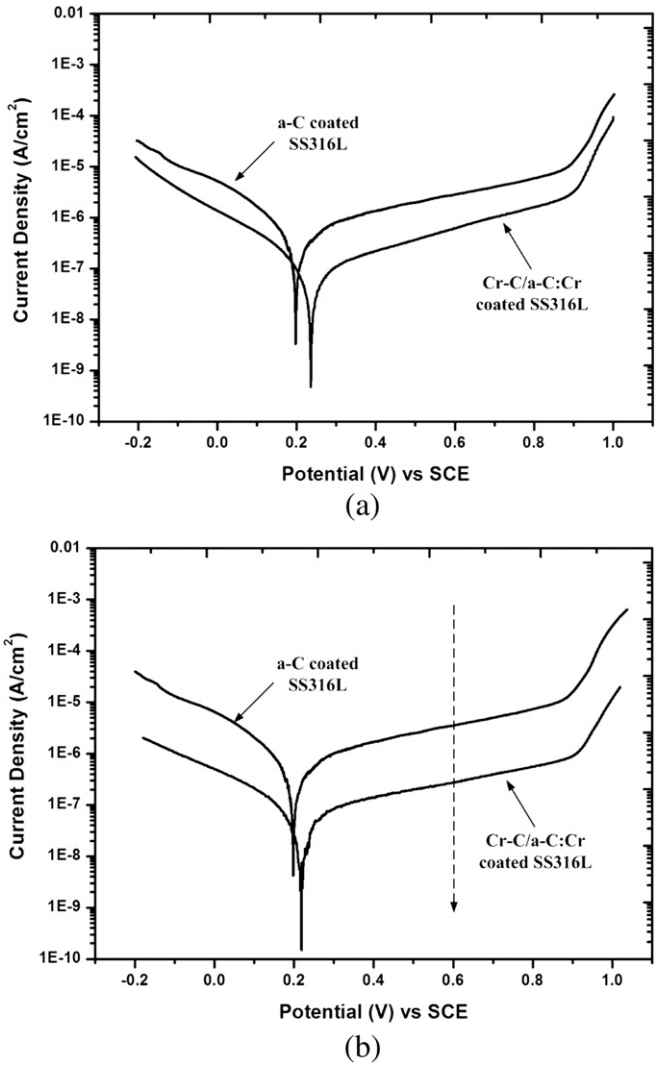

Fig. 9. Polarization curves of the a-C and Cr–C/a-C:Cr coated SS316L samples in 0.5 M H_2SO_4 solution with 5 ppm HF at 70 °C: (a) anode behavior purged with H_2 and (b) cathode behavior bubbled with air.

3.2. Fuel cell characterization

Ex-situ film characterization reveals a potential use of Cr–C/a-C:Cr coated SS316L as bipolar plates undoubtedly. Based on these

Table 3
Metal ions concentration leached from the bare, a-C coated and Cr–C/a-C:Cr coated SS316L samples after 10 h potentiostatic test (ppm).

Sample	Simulated PEMFC cathode environment				
	Fe	Cr	Ni	Mo	Total
Bare SS316L	5.662	1.292	0.836	0.167	7.957
Cr–C/a-C:Cr coated SS316L	0.4295	0.0136	0.0114	0.0051	0.4596
a-C coated SS316L	0.8845	0.0309	0.0268	0.0174	0.9596

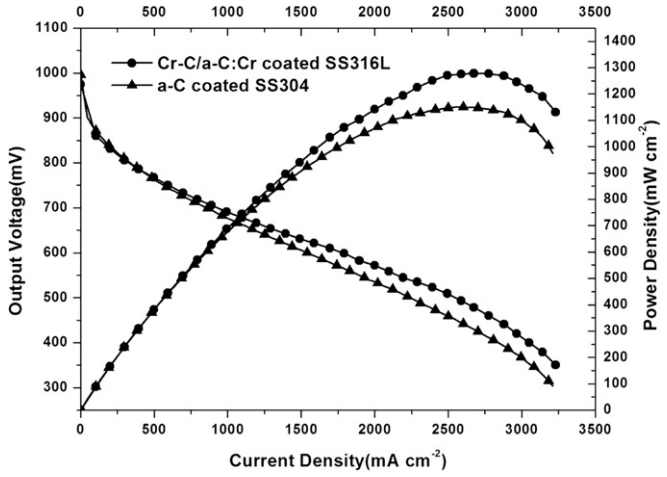

Fig. 10. Initial performance of single cells assembled with a-C coated and Cr–C/a-C:Cr coated SS316L bipolar plates SS304 bipolar plates [20].

experimental results, a single cell with Cr–C/a-C:Cr coated SS316L (FC1) is fabricated and evaluated by polarization curves including the *I–V* and *I–P* curves. Fig. 10 characterizes the initial performance of the single cell after 1 h of activating operation. The performance of the single cell with a-C coated SS304 (FC2) from our previous work is also adopted for comparison [20]. The open circuit voltages (OCV) of the FC1 are almost the same as FC2, being 988.3 mV and 991.6 mV, respectively. Nevertheless, the output performance under high current density shows significant difference. The peak power density of FC1 is 1278.2 mW cm^{-2} at a current density of 2674.1 mA cm^{-2}, while it is 1150.6 mW cm^{-2} for FC2 at 2573.2 mA cm^{-2}. Since the assembly and testing conditions are the same, it is obvious that 11.1% of performance enhancement is achieved by the Cr–C/a-C:Cr coating on SS316L than a-C coating. The trend that the *I–V* curve slope of FC1 is larger than FC2 can be explained by the fact that Cr–C/a-C:Cr coating has lower ICR between bipolar plate and GDL, thus reduces the ohmic losses of PEMFCs.

4. Conclusion

This study develops a multilayered Cr–C/a-C:Cr coating on SS316L sheet as bipolar plates by CFUBMSIP. Material characterization experiments indicate that the thickness of the film is about 1.4 μm and it is mainly composed of the amorphous carbon, metallic Cr phase and chromium carbide phase. Static water contact angle of the film is 89.1° and is beneficial to water management in the PEMFCs stack. ICR between the coated SS316L sheets and carbon paper is only 2.89 mΩ cm^2 at 1.5 MPa. The corrosion potential of coated samples is 0.236 V *vs* SCE in anode environment and the passivation current density is 0.276 μA cm^{-2} at 0.6 V in simulated cathodic environment. Both the electrical conductivity and corrosion resistance obtain performance improvement and meets the DOE's 2020 technical targets. A single cell with Cr–C/a-C:Cr coated SS316L bipolar plates acquires peak power density of 1278.2 mW cm^{-2} at a current density of 2674.1 mA cm^{-2}. Compared to a-C coating developed in our previous work, the Cr–C/a-C:Cr coating achieves 11.1% of performance enhancement and Cr–C/a-C:Cr coated SS316L bipolar plates is more practically applied for commercialization of PEMFCs technology. The single cell with Cr–C/a-C:Cr coated SS316L bipolar plates is still operating continuously in house and the durability performance will be reported in the near future.

Acknowledgement

This work was carried out within the projects supported by the National Natural Science Foundation of China (Nos. 51235008, 51275294, 51121063, and 50930005), the Program of Introducing Talents of Discipline to Universities (No. B06012). It was also supported by National High Technology Research and Development Program of China ("863" program, No. 2011AA11A271). Shanghai Automotive Industry Corporation (SAIC) also gave us financial support through the project "Manufacturing technology of metallic PEMFCs bipolar plates for vehicle applications". Finally, the authors would like to thank Prof. Xun Cai from the School of Materials Science and Engineering, SJTU for helpful discussions.

References

[1] T. Sasabe, S. Tsushima, S. Hirai, Int. J. Hydrogen Energy (2010) 11119–11128.
[2] D.Q. Mei, M. Qian, B.H. Liu, B. Jin, Z.h. Yao, Z.C. Chen, J. Power Sources (2012) 367–376.
[3] C. Du, P.W. Ming, M. Hou, J. Fu, Q. Shen, D. Liang, Y. Fu, X. Luo, Z. Shao, B. Yi, J. Power Sources (2010) 794–800.
[4] Y. Tang, W. Yuan, M.Q. Pan, Z.P. Wan, Int. J. Hydrogen Energy (2010) 9661–9677.
[5] J. Wang, J. Sun, S. Li, Z. Wen, S. Ji, Int. J. Hydrogen Energy (2012) 1140–1144.
[6] M. Luo, C. Huang, W. Liu, Z. Luo, M. Pan, Int. J. Hydrogen Energy (2010) 2986–2993.
[7] W.-L. Wang, S.-M. He, C.-H. Lan, Electrochim. Acta (2012) 30–35.
[8] R.A. Antunes, M.C.L. Oliveira, G. Ett, V. Ett, Int. J. Hydrogen Energy (2010) 3632–3647.
[9] M.C.L. de Oliveira, G. Ett, R.A. Antunes, J. Power Sources (2012) 3–13.
[10] T. Fukutsuka, T. Yamaguchi, S.-I. Miyano, Y. Matsuo, Y. Sugie, Z. Ogumi, J. Power Sources (2007) 199–205.
[11] C.-Y. Chung, S.-K. Chen, P.-J. Chiu, M.-H. Chang, T.-T. Hung, T.-H. Ko, J. Power Sources (2008) 276–281.
[12] Y. Fu, G.Q. Lin, M. Hou, B. Wu, Z. Shao, B. Yi, Int. J. Hydrogen Energy (2009) 405–409.
[13] B. Wu, G.Q. Lin, Y. Fu, M. Hou, B.L. Yi, Int. J. Hydrogen Energy (2010) 13255–13261.
[14] Y.B. Lee, D.S. Lim, Curr. Appl. Phys. (2010) S18–S21.
[15] Y.J. Ren, C.L. Zeng, J. Power Sources (2007) 778–782.
[16] Y. Mori, M. Ueda, M. Hashimoto, Y. Aoi, S. Tanase, T. Sakai, Surf. Coat. Technol. (2008) 4094–4101.
[17] Y. Show, Surf. Coat. Technol. (2007) 1252–1255.
[18] K. Feng, Y. Shen, H.L. Sun, D.A. Liu, Q.Z. An, X. Cai, P.K. Chu, Int. J. Hydrogen Energy (2009) 6771–6777.
[19] W. Jin, K. Feng, Z. Li, X. Cai, L. Yu, D. Zhou, J. Power Sources (2011) 10032–10037.
[20] P.Y. Yi, L.F. Peng, L.Z. Feng, P. Gan, X.M. Lai, J. Power Sources (2010) 7061–7066.
[21] X.C. Chen, Z.J. Peng, Z.Q. Fu, W. Yue, X. Yu, C.B. Wang, Surf. Coat. Technol. (2010) 3319–3325.
[22] P.Y. Yi, L.F. Peng, X.M. Lai, M.T. Li, J. Ni, Int. J. Hydrogen Energy (2012) 11334–11344.
[23] W. Yoon, X. Huang, P. Fazzino, K.L. Reifsnider, M.A. Akkaoui, J. Power Sources (2008) 265–273.
[24] X.M. Lai, D.A. Liu, L.F. Peng, J. Ni, J. Power Sources (2008) 153–159.
[25] P.E. Hovsepian, Y.N. Kok, A.P. Ehiasarian, R. Haasch, J.G. Wen, I. Petrov, Surf. Coat. Technol. (2005) 1572–1579.
[26] E.A. Cho, U.S. Jeon, H.Y. Ha, S.A. Hong, I.H. Oh, J. Power Sources (2004) 178–182.
[27] H. Tawfik, Y. Hung, D. Mahajan, J. Power Sources (2007) 755–767.
[28] U.S. Department of Energy (2011) 3.4-18.